JACS
JOURNAL OF THE AMERICAN CHEMICAL SOCIETY
Article
pubs.acs.org/JACS

# Structural Evidence for a Two-Regime Photobleaching Mechanism in a Reversibly Switchable Fluorescent Protein

Chenxi Duan,[†,‡,§,∥] Virgile Adam,[†,‡,§,∥] Martin Byrdin,[†,‡,§,∥] Jacqueline Ridard,[⊥] Sylvie Kieffer-Jaquinod,[#,$] Cécile Morlot,[†,‡,§] Delphine Arcizet,[†,‡,§,∥] Isabelle Demachy,[⊥] and Dominique Bourgeois*[,†,‡,§,∥]

[†]Université Grenoble Alpes, Institut de Biologie Structurale (IBS), F-38027 Grenoble, France
[‡]CNRS, IBS, F-38027 Grenoble, France
[§]CEA, DSV, IBS, F-38027 Grenoble, France
[∥]Laboratoire de Physiologie Cellulaire et Végétale, IRTSV, CNRS/CEA/INRA/Université Grenoble Alpes, Grenoble, 38054, France
[⊥]Laboratoire de Chimie Physique, UMR 8000, CNRS, Université Paris Sud 11, 91405 Orsay, France
[#]Biologie à Grande Echelle, IRTSV, CEA, Grenoble, France
[$]INSERM, U1038, Grenoble, France

Supporting Information

**ABSTRACT:** Photobleaching, the irreversible photodestruction of a chromophore, severely limits the use of fluorescent proteins (FPs) in optical microscopy. Yet, the mechanisms that govern photobleaching remain poorly understood. In Reversibly Switchable Fluorescent Proteins (RSFPs), a class of FPs that can be repeatedly photoswitched between nonfluorescent and fluorescent states, photobleaching limits the achievable number of switching cycles, a process known as photofatigue. We investigated the photofatigue mechanisms in the protein IrisFP using combined X-ray crystallography, optical *in crystallo* spectroscopy, mass spectrometry and modeling approaches. At laser-light intensities typical of conventional wide-field fluorescence microscopy, an oxygen-dependent photobleaching pathway was evidenced. Structural modifications induced by singlet-oxygen production within the chromophore pocket revealed the oxidation of two sulfur-containing residues, Met159 and Cys171, locking the chromophore in a nonfluorescent protonated state. At laser-light intensities typical of localization-based nanoscopy (>0.1 kW/cm$^2$), a completely different, oxygen-independent photobleaching pathway was found to take place. The conserved Glu212 underwent decarboxylation concomitantly with an extensive rearrangement of the H-bond network around the chromophore, and an sp$^2$-to-sp$^3$ hybridization change of the carbon atom bridging the chromophore cyclic moieties was observed. This two-regime photobleaching mechanism is likely to be a common feature in RSFPs from Anthozoan species, which typically share high structural and sequence identity with IrisFP. In addition, our results suggest that, when such FPs are used, the illumination conditions employed in localization-based super-resolution microscopy might generate less cytotoxicity than those of standard wide-field microscopy at constant absorbed light-dose. Finally, our data will facilitate the rational design of FPs displaying enhanced photoresistance.

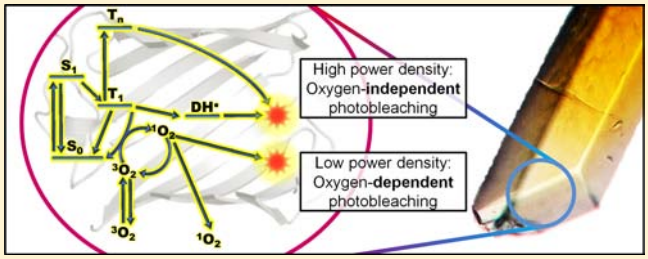


## INTRODUCTION

Recent progresses in fluorescence bioimaging techniques have benefited from the rapid development of a large palette of fluorescent proteins (FPs).[1] However, the limited photostability of FPs has remained a major impediment to their successful use in many approaches including single-molecule, FRET, time-lapse or super-resolution microscopies. FPs typically can only emit ∼10$^5$ photons before their chromophores fall victim to irreversible photodestruction.[2] The detailed photophysical mechanisms leading to photobleaching in FPs remain largely unknown, although some structural insight has been obtained in the case of KillerRed, a highly phototoxic FP.[3−5] Successful efforts to obtain more photostable variants have mainly relied on directed evolution approaches.[2,6−8]

In reversibly switchable fluorescent proteins (RSFPs),[9] photobleaching manifests itself in a process referred to as "photofatigue". RSFPs can be repeatedly photoswitched between a fluorescent (on) and a nonfluorescent (off) state by illumination with visible light of appropriate wavelengths. Photoswitching capabilities are central to a growing number of advanced techniques including a variety of super-resolution modalities,[10−14] photochromic FRET,[15] optical lock-in detection,[16] frequency-domain imaging,[17] optogenetic manipula-

**Received:** July 5, 2013
**Published:** September 23, 2013

   dx.doi.org/10.1021/ja406860e | J. Am. Chem. Soc. 2013, 135, 15841−15850

tion[18] and bio data-storage.[19,20] However, because photobleaching competes with photoswitching, a progressive decrease in fluorescence intensity at each on−off cycle (that is, photofatigue) is observed in ensemble experiments, and at the single molecule level, the number of achievable on−off cycles is limited. Thus, photofatigue fundamentally limits the achievable resolution in nanoscopy approaches such as optically linear fluorescence transition microscopy (RESOLFT)[10] and nonlinear structured illumination microscopy (NSIM),[14] or the contrast enhancement capability in frequency-domain based microscopy schemes.[16,17] Efforts to develop fatigue-resistant RSFPs have been made recently, again essentially based on directed-evolution approaches.[20−22]

Several parameters exert an influence on the photostability of fluorescent proteins. Although the compact FP $\beta$-barrel partially shields the chromophore against molecular oxygen, a number of experimental,[23−25] and theoretical[26,27] investigations concluded that $O_2$ plays an important role in photobleaching of FPs. However, the exact mechanism by which oxygen-dependent chromophore photodestruction occurs has not been directly visualized. Light-induced redox chemistry has also been described to cause a variety of chromophore phototransformations[28] and the photostability of GFP and some derivatives has been shown to depend on the presence of redox-active components in the environment.[29,30] Decarboxylation of the strictly conserved Glu212 (IrisFP numbering, corresponding to Glu222 in GFP) has been described in several cases and is notably involved in photoactivation[31−33] or the formation of super-red species.[34] Such decarboxylation was also observed in experimental conditions not routinely used in fluorescence microscopy, such as at cryogenic temperature[5,35] or under X-ray irradiation.[36,37] The possible involvement of Glu212 decarboxylation in photobleaching under commonly used fluorescence microscopy schemes, nevertheless, has not been documented. In general, it has been repeatedly reported that the photostability of fluorescent proteins may strongly depend on illumination conditions.[2,38−41]

Here, we set out to study the photofatigue mechanism of the biphotochromic RSFP named IrisFP,[42] under experimental conditions typical of wide-field diffraction-limited and super-resolution microscopy. Our previous investigations had revealed the structural and spectroscopic signature of IrisFP in its green and red on-states (chromophore in *cis* conformation), in the corresponding off-states (chromophore in *trans* conformation), and in a reversible dark state (displaying a transiently distorted chromophore geometry consistent with a radical species protonated at atom C$\alpha$ of the methylene bridge[37,43]). In the present work, employing a combination of kinetic X-ray crystallography, *in crystallo* UV−vis absorbance, fluorescence and Raman spectroscopies, mass spectrometry, and molecular dynamics simulations, we discovered two distinct photobleaching mechanisms in IrisFP. The first mechanism is oxygen-independent, whereas the second is oxygen-dependent. A switch from the first to the second mechanism was observed as the illumination power density was decreased from levels typical of localization-based nanoscopy to those of standard wide-field microscopy.

## EXPERIMENTAL PROCEDURES

Experimental procedures are described in details in the Supporting Information.

## RESULTS

**Photofatigue at High Illumination Intensity.** In green IrisFP, illumination by 488-nm (cyan) light isomerizes the fluorescent *cis* anionic chromophore to a *trans* nonfluorescent neutral configuration (quantum yield = $3.2 \times 10^{-3}$). Back-switching to the fluorescent *cis* state is efficiently achieved with 405-nm (violet) light (quantum yield =0.15).[42] We thought of studying the photofatigue of green IrisFP in crystallo under experimental conditions typical of super-resolution PALM microscopy, that is, under relatively high excitation laser power density (~0.1 kW/cm$^2$ at 488 nm, see the Supporting Information, Figure S1A). After 10 min of alternating illumination at 488 and 405 nm, corresponding to about 260 switching cycles, the fluorescence intensity was largely reduced (Figure 1). The decay of the fluorescence envelope appears

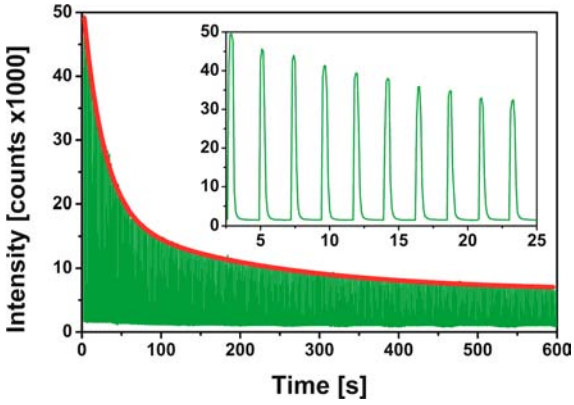


**Figure 1.** Photofatigue fluorescence decay of crystalline IrisFP under high-intensity illumination by 488-nm (~100 W/cm$^2$, continuous) and 405-nm (~1 W/cm$^2$, on for 0.3 s every 2.3 s) laser light. Fluorescence was recorded at 512 nm. The crystal was submitted to 260 switching cycles during 10 min of illumination, which resulted in the loss of ~75% of its initial fluorescence emission. The inset shows an enlarged view of the decay over the first 10 cycles. The fluorescence envelope can be fitted with a biexponential decay model (red trace).

biphasic and can be fitted with a biexponential model in which ~75% of the molecules undergo rapid bleaching and ~25% undergo ~10 times slower bleaching (see discussion in the Supporting Information). Absorbance by the anionic chromophores largely decreased without any increase of the neutral species, suggesting that most molecules were irreversibly bleached (Figure 2A). Similar behavior was observed in solution (Figure S2, Supporting Information).

Experimental difference electron density maps between fatigued and nonfatigued parts of a single crystal (Figure 2C and Table S1, Supporting Information) revealed a complex set of structural modifications confined in the chromophore pocket (Figure S5A, Supporting Information). Strong negative electron density at Glu212 suggested decarboxylation of this residue, as unambiguously confirmed by mass spectrometry analysis (Table S2, Supporting Information). The hydrogen-bond network around the chromophore was largely perturbed, with three water molecules being dislocated and Arg66 and His194 adopting a conformation similar to that found in the *trans* state of the chromophore. The phenolate group of the chromophore appeared largely disordered, together with the hydroxyl group of Ser142 normally H-bonded to the chromophore phenolate. The imidazolinone ring, however, remained planar. These crystallographic data suggest that the chromophore is no longer


dx.doi.org/10.1021/ja406860e | J. Am. Chem. Soc. 2013, 135, 15841−15850

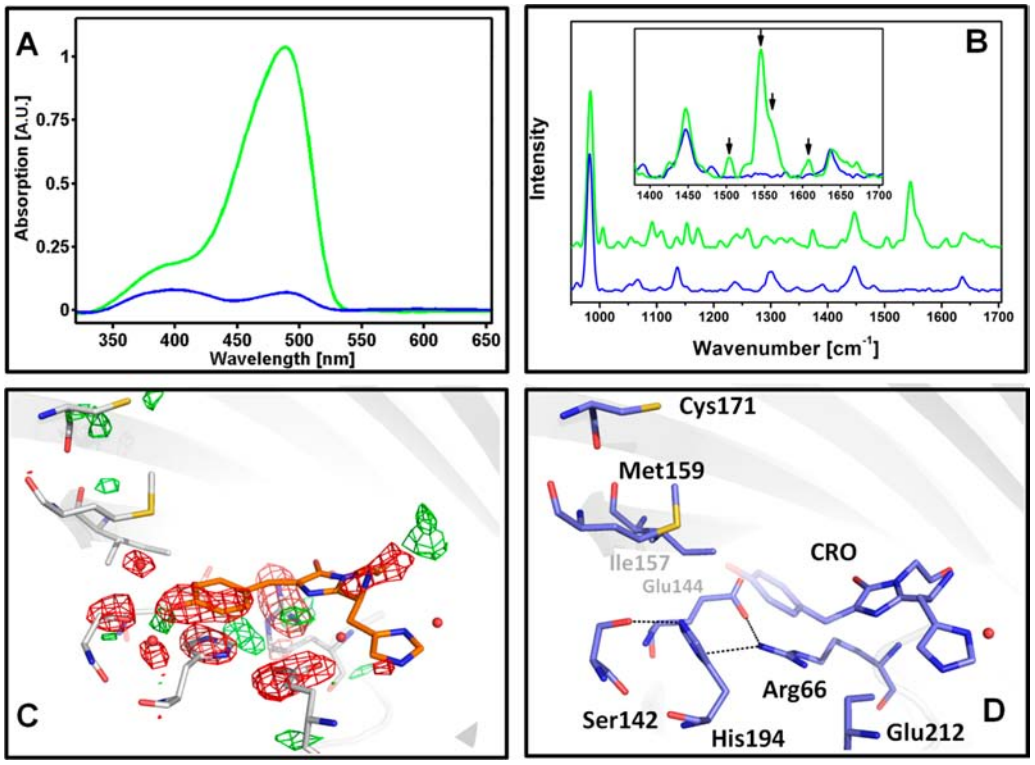


**Figure 2.** (A) Absorption spectra of crystalline IrisFP before (green) and after (blue) high-intensity photobleaching. Both anionic and neutral bands are largely decreased. (B) Raman spectra of crystalline IrisFP before (green) and after (blue) high-intensity photobleaching. The complete disappearance of the 1503, 1545, 1604, and 1564 $cm^{-1}$ bands (inset, arrows) suggests the breakage of the chromophore methylene bridge $\pi$-conjugation (C) NCS-averaged experimental difference electron density map $F_{obs,bleached} - F_{obs,native}$ upon high-intensity photobleaching, overlaid on the crystallographic structure of intact IrisFP (PDB model 2VVH). The chromophore (orange) and the important surrounding residues (gray) in the chromophore pocket are shown. Positive electron density is shown in green (+5 $\sigma$) and negative electron density is shown in red (−5 $\sigma$). (D) Refined model of high-intensity photobleached IrisFP. The chromophore phenolate moiety is represented in dim color to highlight the disorder observed in the electron difference density map. H-bonds are represented with dashed lines, and water molecules as red balls.

properly held in place by the protein matrix and may have lost its electron conjugation.

To gain further insight into the chemical modifications of the chromophore, we performed *in crystallo* Raman spectroscopy of IrisFP crystals illuminated in the same manner. Upon photobleaching, the spectra (Figure 2B) showed considerable modifications (see discussion in the Supporting Information), notably a complete disappearance of the bands at 1503 $cm^{-1}$ and 1545 $cm^{-1}$ (anionic chromophore) and 1564 $cm^{-1}$ and 1604 $cm^{-1}$ (neutral chromophore). The strongly resonance-enhanced band at 1545 $cm^{-1}$ has been assigned to a mode that combines stretching of the C$\alpha$═C5 exocyclic double bond and deformation of the imidazolinone moiety of the chromophore[44] (for chromophore atoms nomenclature, see Scheme S1 in the Supporting Information). In the neutral state of the chromophore, this band is shifted to 1564 $cm^{-1}$, consistent with a more localized electron density in this state. The loss of these bands, together with the vanished UV−vis absorbance, strongly suggests that the C$\alpha$ carbon atom of the chromophore methylene bridge converts from an $sp^2$-hybridized to an $sp^3$-hybridized configuration, possibly as a result of intramolecular electron and proton transfer.[43] Based on these findings, as well as on further molecular dynamics simulations (see below) a model of photodamaged IrisFP was refined (Figure 2D).

Overall, these data suggest that under high-intensity illumination IrisFP suffers from a redox-based photofatigue mechanism, which is associated to decarboxylation of Glu212.

**Photofatigue at Low Illumination Intensity.** Submitting IrisFP crystals to repeated high-intensity laser illumination is a harsh procedure that often compromises their diffraction quality. In an attempt to better preserve the samples, we photofatigued IrisFP crystals at ∼10 times lower power density (∼10 W/$cm^2$ at 488 nm, see the Supporting Information, Figure S1B). After 100 min of alternating cyan and violet illumination (460 switching cycles), fluorescence emission was again largely reduced (Figure 3). However, the fluorescence photofatigue decay profile (Figure 3, red curve) significantly differed from that under high illumination, although a biexponential model was still required to achieve a satisfactory fit (see discussion in the Supporting Information).

To our surprise, the diffraction quality of the crystals was not improved. Instead, it was generally even more degraded. Furthermore, crystallographic analysis revealed neither any substantial structural changes of Glu212 nor any significant distortion or disorder of the chromophore (Figure 4C and Table S1, Supporting Information). Instead, additional positive electron density close to the sulfur atoms of both Met159 and Cys171 was noticed in the difference electron density maps (Figure 4C and Figure S5B, Supporting Information). Absorption spectra of crystals fatigued in this way showed a decreased anionic band but an increased neutral band (Figure 4A). A titration experiment revealed that the p$K_a$ of the photofatigued chromophore increased to ∼12 (Figure S8, Supporting Information) instead of 5.7 under native conditions,[45] suggesting that the chromophore has been trapped in


dx.doi.org/10.1021/ja406860e | J. Am. Chem. Soc. 2013, 135, 15841−15850

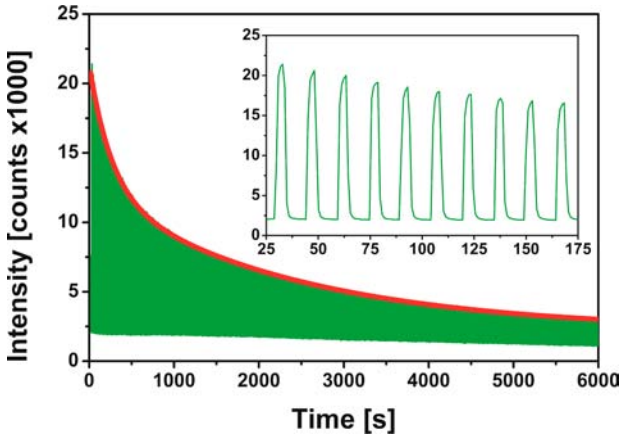


**Figure 3.** Photofatigue fluorescence decay of crystalline IrisFP under low-intensity illumination by 488-nm (~10 W/cm$^2$, continuous) and 405-nm (~0.01 W/cm$^2$, on for 4 s every 12 s) laser light. Fluorescence was recorded at 512 nm. The crystal was submitted to 460 switching cycles during 100 min of illumination, which resulted in the loss of ~90% of its initial fluorescence emission. The inset shows an enlarged view of the decay over the first 10 cycles. The fluorescence envelope can be fitted with a biexponential decay model (red trace).

a nonfluorescent protonated state. Raman spectrometry of a partially fatigued crystal confirmed this finding, displaying an increase of the vibrational bands associated with the neutral chromophore (1564 cm$^{-1}$, 1604 cm$^{-1}$) at the expense of those associated with the anionic chromophore (1503 cm$^{-1}$, 1545 cm$^{-1}$) (Figure 4B), but without signs of a ruptured $\pi$-system. Finally, peptide analysis of a photofatigued sample by mass spectrometry revealed a substantial increase in the level of oxidation of a number of fragments containing methionine, cysteine, and tryptophan residues (Figure S9, Supporting Information). In particular, fragments that contained Met159 had ~320% higher mono-oxidation levels than those of intact IrisFP. Oxidation levels of fragments containing Cys171 were also raised significantly (see Figure S9 caption in the Supporting Information). Conversely, the decarboxylation level of Glu212 remained unaltered as compared to nonbleached IrisFP (Table S2, Supporting Information). These data suggest that, under low-intensity illumination, photofatigue of IrisFP results in sulfoxidation of Met159 and Cys171, followed by oxidation of other residues more remote from the chromophore pocket. Comforted by the mass spectrometry results, we modeled the two positive features near Met159 and Cys171 in the difference electron density map as oxygen atoms covalently bonded to the sulfur atoms of these residues, respectively (Figure 4D). A new water molecule was also modeled next to Met159, above the chromophore hydroxybenzylidene ring. The sulfoxidized Met159 was found to form a tight H-bond (2.8 Å) between the newly added oxygen atom and the presumably protonated chromophore phenol moiety. This tight H-bond is consistent with the extremely high p$K_a$ measured for the fatigued chromophore. Interestingly, the level of Met159 and Cys171 sulfoxidation

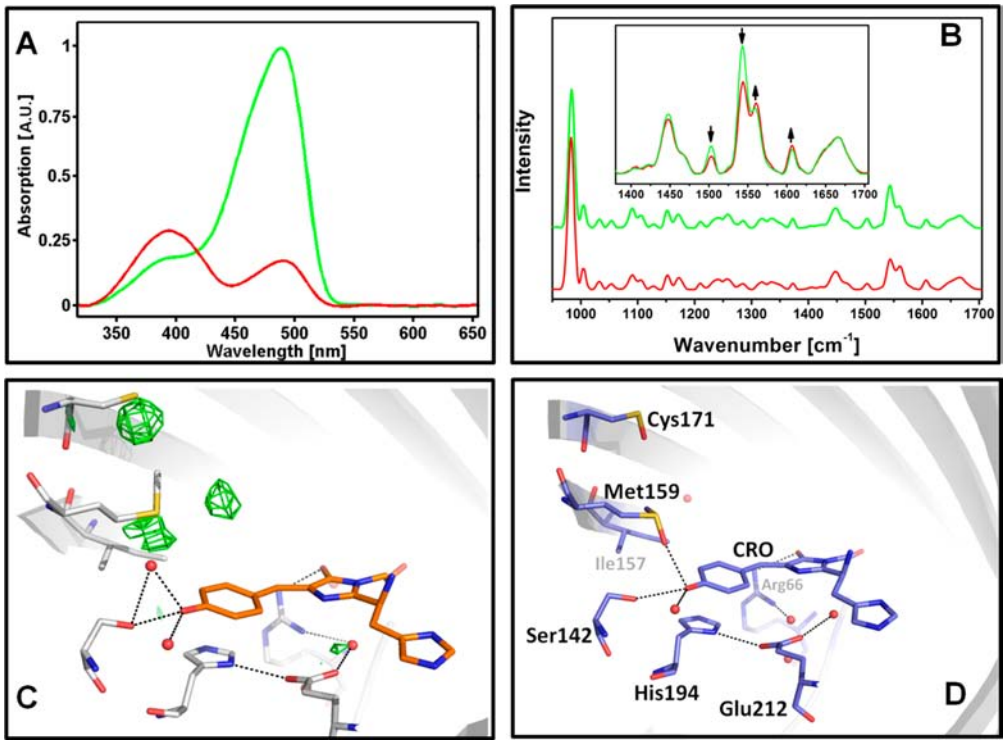


**Figure 4.** (A) Absorption spectra of crystalline IrisFP before (green) and after (red) low-intensity photobleaching. The intensity of the anionic band at 488 nm decreased while that of the neutral band at 390 nm increased. (B) Raman spectra of crystalline IrisFP before (green) and after (red) partial low-intensity photobleaching. The decrease of the 1503 cm$^{-1}$ and 1545 cm$^{-1}$ bands and the increase of the 1604 cm$^{-1}$ and 1564 cm$^{-1}$ bands (inset, arrows) is consistent with a conversion from the anionic to a neutral state of the chromophore without the loss of $\pi$-conjugation (C) NCS-averaged electron difference density map $F_{obs} - F_{calc}$ upon low-intensity photobleaching, overlaid on the crystallographic structure of intact IrisFP (PDB model 2VVH), as in Figure 2C. Positive electron density is shown in green (+5.3 $\sigma$) and negative electron density is shown in red (−5.3 $\sigma$, no feature visible). (D) Refined model of low-intensity photobleaching IrisFP. H-bonds are represented with dashed lines, and water molecules as red balls.


dx.doi.org/10.1021/ja406860e | J. Am. Chem. Soc. 2013, 135, 15841−15850

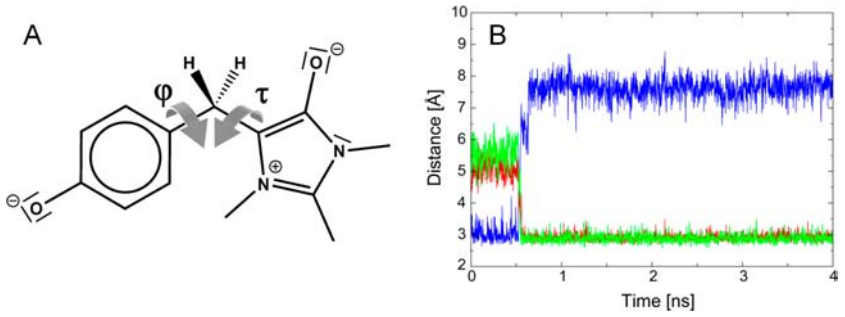


**Figure 5.** (A) Lewis representation of the proposed doubly reduced/protonated chromophore C$\alpha$N photobleached under high-intensity illumination conditions. This structure was used to model the bleached $pBl_{red}$ and $Bl_{red}$ states. (B) MD simulations: time-evolution of characteristic distances between atoms involved in the H-bond network around the IrisFP chromophore pocket, from the $pBl_{red}$ to the $Bl_{red}$ states. Blue: His194(NE2)-Glu144. Red: His194(ND1)-Arg66. Green: His194(NE2)-Ser142.

observed in the electron density maps strongly varied between the four IrisFP monomers. Whereas significant electron densities were observed in monomers A, B, and D, no sign of sulfoxidation could be detected in monomer C (Figure S6A–D, Supporting Information). This difference could be explained by a variable diffusion capacity of oxygen molecules into the chromophore pocket via pores in the IrisFP $\beta$-barrel, probably due to crystal packing effects. In monomers A, B, and D, inspection of the IrisFP static structure showed a pore between the residues Glu140 and Ile196, in the close vicinity of the chromophore phenolate (Figure S6E–H, Supporting Information) at a location previously identified in other FPs such as His148Asp-YFP[46] or the Arthropoda TurboGFP.[47] This pore is occluded in monomer C.

Overall, the data suggest that under low-intensity illumination IrisFP suffers from an oxidation-based photofatigue mechanism, which is initiated by the production of singlet-oxygen within the chromophore pocket.

**Further Insight into IrisFP Photobleaching under High-Intensity Illumination.** The novelty of the decarboxylation-based photofatigue mechanism of IrisFP, its complex structural signature and its potential relevance for high-resolution microscopy prompted us to investigate this mechanism in more details. Notably, we asked the four following questions: (i) Which wavelength (488 or 405 nm) is primarily responsible for photodestruction? (ii) What is the temporal order of the structural events leading to the observed photofatigued structure? (iii) What is the chemical nature of the photobleached chromophore? (iv) Is a two-consecutive-photon absorption process involved?

Question i can be readily answered in the case of low-intensity photobleaching, as the chromophore clearly adopts a *cis* configuration in this bleached state, strongly suggesting that photobleaching results from the absorption of a 488-nm photon. The question is more delicate to answer in the case of high-intensity photobleaching, as two arguments could favor the hypothesis that photodestruction originates from violet light illumination. First, it has been reported that decarboxylation reactions occurring via a Photo-Kolbe mechanism are favored in the UV range.[48] Second, the conformational switch of the His194-Arg66 pair observed in our structure (Figure 2C and 2D) seems at first glance consistent with the chromophore being photobleached in its *trans* configuration by violet light. However, close inspection of the difference electron density map of Figure 2C shows that residue Ile157 maintains a conformation typical of the *cis* chromophoric state.[42] This suggests that the His194-Arg66 switch could be a consequence of photobleaching by cyan light in the *cis* configuration of the chromophore. To test this hypothesis, crystals of green IrisFP were illuminated at 100 K at 488 nm for a prolonged time. At this temperature, chromophore isomerization is prevented, likely due to the lack of sufficient conformational flexibility of the IrisFP chromophore pocket, and thus no switching by *cis–trans* isomerization can occur. Despite a deterioration of the crystalline order resulting from this harsh sample treatment, difference electron density maps clearly showed that 488 nm light is able to induce extensive Glu212 decarboxylation, similarly to 405 nm light (Figure S4, Supporting Information). The conformational switch of the His194-Arg66 pair subsequent to Glu212 decarboxylation in the *cis* chromophoric state was then confirmed by molecular dynamics simulations (see below). These arguments, together with the fact that the sample was exposed to ~600 times more cyan than violet photons, favor the hypothesis that photodestruction upon repeated switching in IrisFP predominantly results from light absorption at 488 nm by the *cis* chromophore.

We next attempted to disentangle the order of the structural events leading to chromophore destruction (question ii) by collecting a high-quality structure of IrisFP en-route to photobleaching. Knowing that X-rays efficiently induce IrisFP photobleaching through Glu212 decarboxylation,[37] we reasoned that collecting a pair of high-resolution crystallographic structures at 100K at different X-ray doses might uncover structural differences representative of early events along the photobleaching pathway. The results, presented in Figure S7 (Supporting Information) (see also Tables S1 and S3, Supporting Information), reveal decarboxylation of Glu212 as well as the disappearance of several water molecules participating in the hydrogen bond network surrounding the chromophore. However, instead of the disorder of the phenolate moiety observed in the photofatigued structure, the chromophore exhibits a clear distortion with an upward tilt of the chromophore phenolate and a downward bend of the methylene bridge. This distortion is also consistent with $sp^3$-hybridization of the $C_\alpha$ carbon atom (Figure 2D). Furthermore, His194 and Arg66 are not significantly displaced as compared to their native conformation. If we admit that photobleaching pathways induced by high-intensity visible and X-ray light are both initiated by redox processes leading to Glu212 decarboxylation, it is reasonable to associate these structural changes with an early intermediate state along the high-intensity photofatigue pathway.

To further investigate whether the X-ray bleached cryo-structure is a plausible intermediate state along the high-

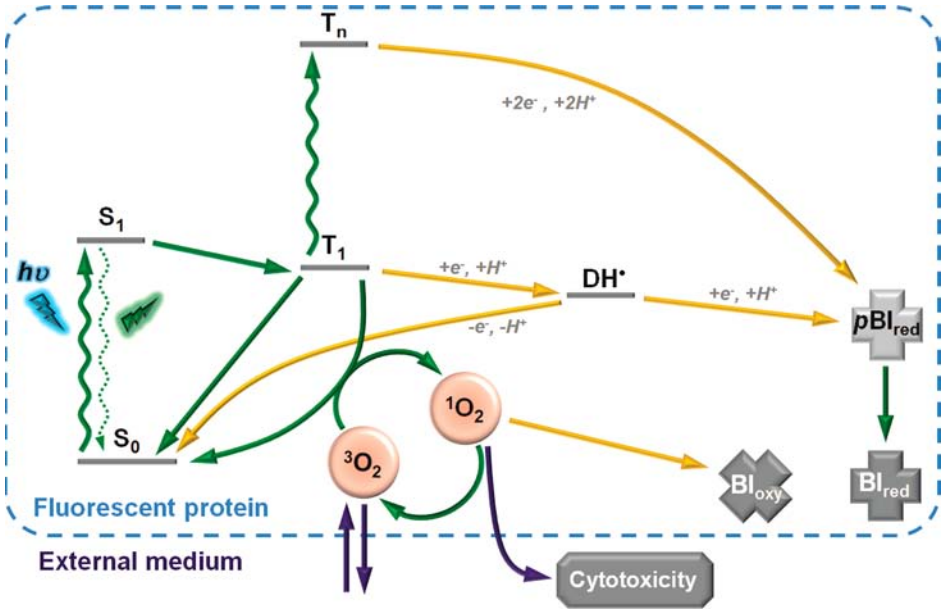


**Figure 6.** Proposed photophysical scheme for a two-regime photobleaching in IrisFP. Yellow arrows represent chemical steps involving electron/proton transfer or oxidation reactions. Blue arrows represent entry/exit of oxygen species.

intensity photofatigue pathway, we conducted molecular dynamics simulations using software specifically tailored for fluorescent proteins simulations.[49] These simulations also allowed us to examine the chemical nature of the fatigued chromophore (question iii). Starting from the putative intermediate state with the chromophore adopting various chemical structures, we analyzed whether or not the IrisFP conformation evolved toward the experimentally observed fatigued structure. In order to ensure the $sp^3$-character of the C$\alpha$ atom revealed by Raman spectroscopy while excluding an unstable radical state of the fatigued chromophore, the latter must be considered as formally reduced by two hydrogen atoms. Among all available choices tested (Figure S10, Table S4, Supporting Information), the reduced structure protonated at positions C$\alpha$ and N4 (referred to as C$\alpha$N) was found to be the only one compatible with our experimental data (Figure 5A). Protonation at other positions either altered the planar character of the imidazolinone ring or weakened the hydrogen bond between that ring and Arg91 (see further discussion in the Supporting Information). Using structure C$\alpha$N in our MD simulations, we noticed that the conformational switch of His194 and Arg66 to their positions observed in the fatigued structure occurred within a nanosecond (Figure 5B and Figure S14, Supporting Information). Furthermore, large fluctuations of the chromophore torsions around the C$\alpha$ atom were observed afterward (the 80% confidence interval of the dihedral $\tau$ angle ranged from $-5°$ to $55°$), reflecting the interplay between the intramolecular energy landscape of the reduced chromophore C$\alpha$N (Figure S11, Supporting Information) and the decreased constraints due to the protein environment. These fluctuations are consistent with the phenolate disorder observed experimentally.

Finally, in order to investigate whether the high-intensity bleaching mechanism involves a two-consecutive-photon absorption process (question iv), we measured the initial photofatigue rate as a function of the illumination power density in the absence of oxygen (Figure S3, Supporting Information). The results confirm that $O_2$ is indeed not required in this mechanism. The best linear fit to a double-logarithmic plot of the data showed a slope of $1.8 \pm 0.3$ (Figure S3, Supporting Information), indicating a mechanism mainly involving two photons with a possible weak residual from a one-photon contribution.

## ■ DISCUSSION

Our study of the photofatigue mechanism of the reversibly switchable protein IrisFP reveals a two-regime photodestruction pathway. At illumination intensities of ~100 W/cm$^2$, photobleaching of IrisFP involves decarboxylation of Glu212 probably via electron transfer to the chromophore in a photo-Kolbe reaction.[31,48] We propose that this leads to a prebleached dark state, represented by the cryo-trapped structure of Figure S7 (Supporting Information), in which the chromophore is already reduced and protonated at the C$\alpha$ atom and at the N4 nitrogen atom. In this state, denoted $pBI_{red}$, the chromophore has lost its electron conjugation and adopts a tilted geometry. (Note that $pBI_{red}$ differs from the blinked radical state $DH^{\bullet}$ described earlier by us.[43]) Subsequently, while the chemical structure of the chromophore does not evolve further, the hydrogen bond network surrounding it collapses, and the His194-Arg66 pair flips to a conformation resembling that of IrisFP in its switched-off state. The phenolate moiety of the chromophore loses its anchoring to the protein matrix, resulting in large fluctuations of the $\tau$ and $\varphi$ dihedral angles. A complete loss of absorbance and fluorescence is thus observed in this bleached state, referred to as $BI_{red}$, and the presence of oxygen is not required.

At illumination intensities ten times lower (~10 W/cm$^2$), a completely different scenario takes place. The chromophore reacts in its triplet state $T_1$ with molecular oxygen to produce singlet oxygen $^1O_2$. We propose that singlet oxygen then rapidly reacts with the nearby Met159 and a water molecule to produce sulfoxidized-Met159 and hydrogen peroxide $H_2O_2$.[50] $H_2O_2$ in turn attacks Cys171 to give sulfoxidized Cys171 and a hydroxyl molecule.[50] Because the S−O bond in a sulfoxidized methionine is highly polarized, with partial negative charge on


dx.doi.org/10.1021/ja406860e | J. Am. Chem. Soc. 2013, 135, 15841−15850

the oxygen atom, the chromophore is trapped in a protonated state due to the establishment of a strong H-bond interaction. Loss of fluorescence is observed, but partial absorption by the neutral chromophore is maintained. Alternatively to oxidizing Met159 and Cys171, singlet oxygen may also diffuse further throughout the IrisFP matrix and attack more remote amino acids, as revealed by mass spectrometry. We refer to either of these oxygen dependent bleached states as $Bl_{oxy}$. Singlet oxygen may also undergo a different fate: it can escape into the solvent and generate cytotoxicity. This is consistent with the estimated $^1O_2$ lifetime and diffusion length in cells of 250 ns and 45 nm, respectively.[51] Diffusion out of the IrisFP $\beta$-barrel could occur via the pore identified in this work, or through other pores opening transiently that will necessitate future investigations by molecular dynamics simulations.[26,27]

Sulfur-containing residues are major targets of reactive oxygen species (ROS) and are most susceptible to oxidation.[52] Notably, methionine oxidation by singlet oxygen has been described in the context of chromophore assisted light inactivation (CALI), typically resulting in enzyme inactivation.[53] Here, low-intensity photobleaching of IrisFP can be viewed as a special case of intramolecular CALI. We note that it is unlikely that methionine sulfoxide reductases, which are enzymes known to revert methionine sulfoxidation[54] would salvage IrisFP fluorescence, because Met159 is buried into the $\beta$-barrel. Further oxidation of remote sensitive residues could also be associated with a loss of fluorescence possibly linked to partial unfolding of the IrisFP $\beta$-barrel, in turn corroborating the loss of diffraction observed in crystals treated with prolonged low-intensity light. This observation is reminiscent of the loss of enzymatic activity observed in enzymes submitted to a high-level of oxidation by ROS,[50,55] and it is consistent with the loss of fluorescence observed in other FPs submitted to ROS by pulse radiolysis.[56]

The photophysical scheme of Figure 6 recapitulates the proposed photobleaching pathways. Upon excitation, the ground-state singlet chromophore $S_0$ reaches the first electronically excited state $S_1$, from which it can either fluoresce, deactivate nonradiatively (through isomerization, giving rise to off-switching), or undergo intersystem crossing to the long-lived triplet state $T_1$. From $T_1$, a number of possible pathways can be envisaged. $T_1$ can relax to $S_0$ either spontaneously or, more efficiently, by triplet−triplet quenching if molecular oxygen is present near the chromophore. This results in the production of $^1O_2$ which may, as described above, attack the fluorescent protein or escape into the medium. The photofatigued state $Bl_{oxy}$ is produced. Alternatively, the high oxidation potential of the excited chromophore may drive electron transfer from Glu212 without the need for oxygen, leading to the nonfluorescent prebleached state $pBl_{red}$ from which the photofatigued state $Bl_{red}$ occurs.

It is interesting to determine which factors control the switch from one photobleaching regime to the other. Two hypotheses can be proposed. First, the entry rate of molecular oxygen into the IrisFP $\beta$-barrel could play a role. A slow $O_2$ entry rate relative to the rate of photon absorption would disfavor the reaction of the excited IrisFP chromophore with oxygen, leaving redox chemistry as the dominant route to photobleaching. Second, as strongly suggested by our data (Figure S3, Supporting Information), the onset of redox photobleaching at high intensity could result from a mechanism relying on the consecutive absorption of two photons. The increase of the $T_1$ lifetime while oxygen is absent from the chromophore pocket would further boost such mechanism. In order to test these hypotheses, the complete kinetic model illustrated in Figure S15 (Supporting Information) was challenged by simulations predicting the relative fraction of the two photofatigued species $Bl_{red}$ and $Bl_{oxy}$ as a function of the applied laser intensity, assuming realistic rates for entry/exit of oxygen in/from the chromophore pocket (see discussion in the Supporting Information and Figure S16). The model consistently predicts dominant oxygen-dependent and oxygen-independent photobleaching pathways under the experimental low- and high-intensity illumination conditions, respectively. We propose that the photobleached state $Bl_{red}$ can be reached via one- or two-consecutive-photon excitation. In the first case, the radical state $DH^{\bullet}$ could be involved, as suggested by our previous simulations using QM/MM approaches.[43] In the second case, absorption of the second photon could take place in $T_1$ or another state of the chromophore with micro- to millisecond lifetime, thus accelerating formation of $Bl_{red}$ at high excitation rates. The existence of a two-consecutive-photon absorption route leading to Glu222 decarboxylation has been noticed in GFP[57] and is consistent with the high laser intensities observed to build-up the super-red species in DsRed.[34] Furthermore, by analogy to the results found in GFP,[57] it may be speculated that conventional two-photon-excitation schemes, in view of the high laser power-densities used, could favor the oxygen-independent bleaching pathway.

In the crystalline state, assuming a typical concentration of oxygen of 200 $\mu$M, there is a large excess of IrisFP monomers (>100). Assuming a bulk diffusion coefficient of $2 \times 10^{-5}$ cm$^2$/s, a single molecule of $O_2$ is able to explore only ~20 unit cells in a microsecond. Thus, it is likely that the rate at which oxygen molecules penetrate into a given crystalline IrisFP monomer is lower than the excitation rate of the chromophore, at least under our high-intensity illumination conditions ($5 \times 10^4$ s$^{-1}$). In solution samples or in biological cells this situation might differ, with more molecular oxygen available per fluorophore. This may possibly shift upward the intensity threshold between the two photobleaching pathways. More generally, we expect this threshold to depend not only on the fluorescent protein and molecular oxygen concentrations but also on the redox environment, as well as on other parameters such as pH, viscosity of the medium, or even the nature of fusion constructs.

Photo-Kolbe reactions in fluorescent proteins have been described several times.[31−33,48,58] The invoked mechanism, however, always leaves the chromophore intact. Indeed, it is generally proposed that following electron transfer from Glu212 to the chromophore, an electron (and proton) is transferred back from the chromophore to the $CH_2^{\bullet}$ radical of the decarboxylated Glu212. By contrast, the chromophore of IrisFP is chemically altered, with the methylene bridge ending up in an sp$^3$-hybridized state as demonstrated by Raman spectroscopy. The photobleached chromophore is thus likely to be photochemically reduced, which implies the net transfer of two electrons and two protons. Our MD simulations favor such a process, suggesting the formation of a zwitterionic imidazolinone ring in which the oxygen atom is negatively charged and stabilized by two H-bonds to the guanidinium groups of Arg66 and Arg91 while the N4 nitrogen atom is protonated and positively charged. Whereas the proton ending up on the C$\alpha$ carbon could originate from Arg66,[43] we speculate that the second electron and proton could be


dx.doi.org/10.1021/ja406860e | J. Am. Chem. Soc. 2013, 135, 15841−15850

provided by a reducing molecule in the surrounding medium.[29] Further studies will be needed, however, to precisely unravel the redox mechanism allowing these transfers.

Studying the photobleaching mechanisms of RSFPs is important because these markers play an increasing role in several advanced fluorescence microscopy applications. It could be argued, however, that the photoswitching capabilities of RSFPs complicate the investigation of irreversible photodestruction processes. On the contrary, and consistently with previous work,[41] we propose that the investigation of photobleaching pathways through repeated photoswitching provides the advantage that uncontrolled accumulation of reversible dark states ("shelving")[2] is largely reduced: the overall slow photofatigue of RSFPs facilitates the recovery of thermally unstable dark states, and repeated illumination by 405 nm light often promotes fast recovery of light-sensitive dark states, as is the case for the main *trans*-isomeric off state. Overall, studying photobleaching of RSFPs facilitates the decoupling of irreversible and reversible photophysical processes.

The photobleaching mechanisms described here for IrisFP might be conserved in other photoconvertible and photoswitchable fluorescent proteins derived from Anthozoan species such as Dronpa, mTFP0.7, Kaede, EosFP, Dendra2, and their variants.[39] Indeed, all these proteins display very similar structural organizations of their chromophore pocket, with nearly identical hydrogen bond networks involving Glu212, His194, Arg66, and Glu144. Their sequence identity and global structural similarity is also high, suggesting the possibility of a common pathway for oxygen diffusion toward the chromophore and/or common redox mechanisms. Moreover, all these proteins, except mTFP0.7, contain a methionine at position 159. The observation of a trapped neutral chromophore upon Met159 sulfoxidation might therefore be a general feature of this family of proteins. We note that, in the context of the present study, the presence of this residue at this position can be considered as a fortunate feature that allowed us to provide the first structural evidence of singlet oxygen production within a FP chromophore pocket. Interestingly, during the directed evolution of mCherry from mRFP1, it was reported that the mutation Met163Gln was entirely responsible for the 10-fold enhanced photostability of mCherry.[2] This finding could relate to our observations in IrisFP, although recent molecular dynamics simulations proposed that this mutation essentially served to block the entry of molecular oxygen within the barrel.[27]

In general, the photobleaching mechanisms observed in IrisFP are unlikely to apply to Hydrozoan RSFPs such as rsEGFP.[20,21] While oxygen diffusion pathways probably differ, Glu212 decarboxylation in Hydrozoan FPs typically induces photoactivation rather than photobleaching. Nevertheless, competing photobleaching routes probably also exist in Hydrozoan RSFPs and would deserve investigations similar to those described in this work. Likewise, non-RSFPs of Anthozoan origin are likely to exhibit yet different photobleaching mechanisms. In the red fluorescent protein KillerRed, for which structures of photobleached states under low intensity illumination have been published,[3,4] the chromophore was found either disordered[3] or distorted,[4] possibly consistent with $sp^3$-hybridization of the methylene bridge, and no substantial modifications of the chromophore environment was noticed. These differences with our low-intensity IrisFP bleached structure might arise from a type I photosensitization mechanism in KillerRed[3] versus a type II mechanism in IrisFP and be a consequence of the different chromophore structures and environments in the two proteins.

Our results provide some of the molecular basis required for the rational design of more photoresistant Anthozoan RSFPs. For example, in IrisFP, mutations Met159Ala[45] or Glu212Gln[59] could be carried out and their effect on photobleaching investigated, with the potential caveat that mutations enhancing photoresistance may also modify important properties such as photoswitching yields or maturation efficiency. Further directed-evolution based engineering of electron transfer pathways and oxygen entry routes will probably be required to obtain optimal photoresistant variants.

## ■ CONCLUSION

Despite considerable advances in fluorescent proteins research in the recent past, the high susceptibility of FPs to irreversible photobleaching still remains a major bottleneck to their use in advanced microscopy applications. Here, we have explored the photobleaching mechanisms in IrisFP, a representative of the important class of reversibly switchable fluorescent proteins. Under low-intensity illumination (~0.01 kW/cm$^2$) typical of standard wide-field fluorescence microscopy, an oxygen-dependent mechanism dominates, that damages the IrisFP chromophore environment mainly through sulfoxidation reactions and releases singlet oxygen in the medium. Under high-intensity illumination (~0.1 kW/cm$^2$) approaching laser-light levels used in localization-based super-resolution microscopy, an oxygen-independent mechanism takes over, that damages the chromophore itself via decarboxylation of the strictly conserved Glu212.

As a consequence of this work we speculate that high-intensity illumination of Anthozoan phototransformable FPs might generate less cytotoxicity than low-intensity illumination at constant integrated dose. This prediction is consistent with previous findings that light-induced damage of cellular samples labeled with fluorescent proteins mostly originates from ROS released by the fluorescent markers under typical widefield illumination regimes.[60,61] However, at high-intensity, additional effects due to, e.g., singlet oxygen release by endogenous chromophores (such as flavins) and rapid depletion of ROS scavenging cellular components (such as glutathione) may play an adverse role. Overall, our results might be related to the observation that prolonged PALM illumination of Anthozoan FPs generally induces tolerable phototoxicity in live cells,[62−65] but call for further quantitative investigations of the light-intensity dependence of cytotoxic effects in biological samples. The two-regime photobleaching mechanism characterized in this work may also play a role in the frequently observed discrepancy between bleaching kinetics measured under a variety of conditions, typically low versus high intensity wide-field or wide-field versus confocal. In the latter case, however, the short illumination dwell-times and typically much higher instantaneous power densities (>10 kW/cm$^2$) probably call for yet other photobleaching mechanisms to be explored in the future.

## ■ ASSOCIATED CONTENT

### Supporting Information

Materials and methods for crystal growth, X-ray data collection and structure determination, photobleaching procedures, optical spectroscopy and mass spectrometry, quantum mechanics and molecular dynamics simulations. Discussions

of laser beam heterogeneity, QM/MD simulations, modeling of kinetic scheme, Raman spectra from photobleached crystals. This material is available free of charge via the Internet at http://pubs.acs.org.

## AUTHOR INFORMATION


### Corresponding Author

dominique.bourgeois@ibs.fr


### Notes

The authors declare no competing financial interest

## ACKNOWLEDGMENTS

The ESRF and SLS synchrotron facilities are acknowledged for providing beamtime. We thank Martin Fuchs, Guillaume Pompidor, and Florian Dworkowski for help in X-ray data collection at the SLS, Aline Faro for scientific discussions, and David von Stetten for support in using the Cryobench laboratory of the ESRF. We acknowledge technical help by Laure Roux, Jérémie Gaillard and Christophe Guerin. We thank Gabriella Jonasson and Bernard Lévy for fruitful discussions and invaluable help. D.B. acknowledges financial support by the ANR (ANR-2011-BSV5-012-01 NOBLEACH). This work used the platforms of the Grenoble Instruct center (ISBG; UMS 3518 CNRS-CEA-UJF-EMBL) with support from FRISBI (ANR-10-INSB-05-02) and GRAL (ANR-10-LABX-49-01) within the Grenoble Partnership for Structural Biology (PSB). This work was granted access to the HPC resources of CINES under the allocation 2012-c2012086318 made by GENCI (Grand Equipement National de Calcul Intensif).

## REFERENCES


(1) Dedecker, P.; De Schryver, F. C.; Hofkens, J. *J. Am. Chem. Soc.* **2013**, *135*, 2387.

(2) Shaner, N. C.; Lin, M. Z.; McKeown, M. R.; Steinbach, P. A.; Hazelwood, K. L.; Davidson, M. W.; Tsien, R. Y. *Nat. Methods* **2008**, *5*, 545.

(3) Pletnev, S.; Gurskaya, N. G.; Pletneva, N. V.; Lukyanov, K. A.; Chudakov, D. M.; Martynov, V. I.; Popov, V. O.; Kovalchuk, M. V.; Wlodawer, A.; Dauter, Z.; Pletnev, V. *J. Biol. Chem.* **2009**, *284*, 32028.

(4) Carpentier, P.; Violot, S.; Blanchoin, L.; Bourgeois, D. *FEBS Lett.* **2009**, *583*, 2839.

(5) de Rosny, E.; Carpentier, P. *J. Am. Chem. Soc.* **2012**, *134*, 18015.

(6) Ai, H. W.; Henderson, J. N.; Remington, S. J.; Campbell, R. E. *Biochem. J.* **2006**, *400*, 531.

(7) Subach, O. M.; Cranfill, P. J.; Davidson, M. W.; Verkhusha, V. V. *PLoS One* **2011**, *6*, e28674.

(8) Christie, J. M.; Hitomi, K.; Arvai, A. S.; Hartfield, K. A.; Mettlen, M.; Pratt, A. J.; Tainer, J. A.; Getzoff, E. D. *J. Biol. Chem.* **2012**, *287*, 22295.

(9) Bourgeois, D.; Adam, V. *IUBMB Life* **2012**, *64*, 482.

(10) Hofmann, M.; Eggeling, C.; Jakobs, S.; Hell, S. W. *Proc. Natl. Acad. Sci. U.S.A.* **2005**, *102*, 17565.

(11) Dedecker, P.; Hotta, J.; Flors, C.; Sliwa, M.; Uji-i, H.; Roeffaers, M. B.; Ando, R.; Mizuno, H.; Miyawaki, A.; Hofkens, J. *J. Am. Chem. Soc.* **2007**, *129*, 16132.

(12) Bock, H.; Geisler, C.; Wurm, C. A.; Von Middendorff, C.; Jakobs, S.; Schonle, A.; Egner, A.; Hell, S. W.; Eggeling, C. *Appl. Phys. B-Lasers Opt.* **2007**, *88*, 161.

(13) Shroff, H.; Galbraith, C. G.; Galbraith, J. A.; White, H.; Gillette, J.; Olenych, S.; Davidson, M. W.; Betzig, E. *Proc. Natl. Acad. Sci. U.S.A.* **2007**, *104*, 20308.

(14) Rego, E. H.; Shao, L.; Macklin, J. J.; Winoto, L.; Johansson, G. A.; Kamps-Hughes, N.; Davidson, M. W.; Gustafsson, M. G. *Proc. Natl. Acad. Sci. U.S.A.* **2011**, *109*, E135.

(15) Subach, F. V.; Zhang, L. J.; Gadella, T. W. J.; Gurskaya, N. G.; Lukyanov, K. A.; Verkhusha, V. V. *Chem. Biol.* **2010**, *17*, 745.

(16) Marriott, G.; Mao, S.; Sakata, T.; Ran, J.; Jackson, D. K.; Petchprayoon, C.; Gomez, T. J.; Warp, E.; Tulyathan, O.; Aaron, H. L.; Isacoff, E. Y.; Yan, Y. L. *Proc. Natl. Acad. Sci. U. S. A.* **2008**, *105*, 17789.

(17) Tian, Z.; Li, A. D. *Acc. Chem. Res.* **2013**, *46*, 269.

(18) Zhou, X. X.; Chung, H. K.; Lam, A. J.; Lin, M. Z. *Science* **2012**, *338*, 810.

(19) Adam, V.; Mizuno, H.; Grichine, A.; Hotta, J. I.; Yamagata, Y.; Moeyaert, B.; Nienhaus, G. U.; Miyawaki, A.; Bourgeois, D.; Hofkens, J. *J. Biotechnol.* **2010**, *149*, 289.

(20) Grotjohann, T.; Testa, I.; Leutenegger, M.; Bock, H.; Urban, N. T.; Lavoie-Cardinal, F.; Willig, K. I.; Eggeling, C.; Jakobs, S.; Hell, S. W. *Nature* **2011**, *478*, 204.

(21) Grotjohann, T.; Testa, I.; Reuss, M.; Brakemann, T.; Eggeling, C.; Hell, S. W.; Jakobs, S. *Elife* **2012**, *1*, e00248.

(22) Chang, H.; Zhang, M.; Ji, W.; Chen, J.; Zhang, Y.; Liu, B.; Lu, J.; Zhang, J.; Xu, P.; Xu, T. *Proc. Natl. Acad. Sci. U.S.A.* **2012**, *109*, 4455.

(23) Greenbaum, L.; Rothmann, C.; Lavie, R.; Malik, Z. *Biol. Chem.* **2000**, *381*, 1251.

(24) Jimenez-Banzo, A.; Nonell, S.; Hofkens, J.; Flors, C. *Biophys. J.* **2008**, *94*, 168.

(25) Jimenez-Banzo, A.; Ragas, X.; Abbruzzetti, S.; Viappiani, C.; Campanini, B.; Flors, C.; Nonell, S. *Photochem. Photobiol. Sci.* **2010**, *9*, 1336.

(26) Roy, A.; Carpentier, P.; Bourgeois, D.; Field, M. *Photochem. Photobiol. Sci.* **2010**, *9*, 1342.

(27) Regmi, C. K.; Bhandari, Y. R.; Gerstman, B. S.; Chapagain, P. P. *J. Phys. Chem. B* **2013**, *117*, 2247.

(28) Subach, F. V.; Verkhusha, V. V. *Chem. Rev.* **2012**, *112*, 4308.

(29) Bogdanov, A. M.; Bogdanova, E. A.; Chudakov, D. M.; Gorodnicheva, T. V.; Lukyanov, S.; Lukyanov, K. A. *Nat. Methods* **2009**, *6*, 859.

(30) Malkani, N.; Schmid, J. A. *PLoS One* **2011**, *6*.

(31) van Thor, J. J.; Gensch, T.; Hellingwerf, K. J.; Johnson, L. N. *Nat. Struct. Biol.* **2002**, *9*, 37.

(32) Henderson, J. N.; Gepshtein, R.; Heenan, J. R.; Kallio, K.; Huppert, D.; Remington, S. J. *J. Am. Chem. Soc.* **2009**, *131*, 4176.

(33) Subach, F. V.; Malashkevich, V. N.; Zencheck, W. D.; Xiao, H.; Filonov, G. S.; Almo, S. C.; Verkhusha, V. V. *Proc. Natl. Acad. Sci. U.S.A.* **2009**, *106*, 21097.

(34) Habuchi, S.; Cotlet, M.; Gensch, T.; Bednarz, T.; Haber-Pohlmeier, S.; Rozenski, J.; Dirix, G.; Michiels, J.; Vanderleyden, J.; Heberle, J.; De Schryver, F. C.; Hofkens, J. *J. Am. Chem. Soc.* **2005**, *127*, 8977.

(35) van Thor, J. J.; Georgiev, G. Y.; Towrie, M.; Sage, J. T. *J. Biol. Chem.* **2005**, *280*, 33652.

(36) Royant, A.; Noirclerc-Savoye, M. *J. Struct. Biol.* **2011**, *174*, 385.

(37) Adam, V.; Carpentier, P.; Violot, S.; Lelimousin, M.; Darnault, C.; Nienhaus, G. U.; Bourgeois, D. *J. Am. Chem. Soc.* **2009**, *131*, 18063.

(38) Shcherbo, D.; Murphy, C. S.; Ermakova, G. V.; Solovieva, E. A.; Chepurnykh, T. V.; Shcheglov, A. S.; Verkhusha, V. V.; Pletnev, V. Z.; Hazelwood, K. L.; Roche, P. M.; Lukyanov, S.; Zaraisky, A. G.; Davidson, M. W.; Chudakov, D. M. *Biochem. J.* **2009**, *418*, 567.

(39) Chudakov, D. M.; Matz, M. V.; Lukyanov, S.; Lukyanov, K. A. *Physiol. Rev.* **2010**, *90*, 1103.

(40) Carlton, P. M.; Boulanger, J.; Kervrann, C.; Sibarita, J. B.; Salamero, J.; Gordon-Messer, S.; Bressan, D.; Haber, J. E.; Haase, S.; Shao, L.; Winoto, L.; Matsuda, A.; Kner, P.; Uzawa, S.; Gustafsson, M.; Kam, Z.; Agard, D. A.; Sedat, J. W. *Proc. Natl. Acad. Sci. U.S.A.* **2010**, *107*, 16016.

(41) Dean, K. M.; Lubbeck, J. L.; Binder, J. K.; Schwall, L. R.; Jimenez, R.; Palmer, A. E. *Biophys. J.* **2011**, *101*, 961.

(42) Adam, V.; Lelimousin, M.; Boehme, S.; Desfonds, G.; Nienhaus, K.; Field, M. J.; Wiedenmann, J.; McSweeney, S.; Nienhaus, G. U.; Bourgeois, D. *Proc. Natl. Acad. Sci. U.S.A.* **2008**, *105*, 18343.

(43) Roy, A.; Field, M. J.; Adam, V.; Bourgeois, D. *J. Am. Chem. Soc.* **2011**, *133*, 18586.

(44) He, X.; Bell, A. F.; Tonge, P. J. *J. Phys. Chem. B* **2002**, *106*, 6056.

(45) Adam, V.; Moeyaert, B.; David, C. C.; Mizuno, H.; Lelimousin, M.; Dedecker, P.; Ando, R.; Miyawaki, A.; Michiels, J.; Engelborghs, Y.; Hofkens, J. *Chem. Biol.* **2011**, *18*, 1241.
(46) Wachter, R. M.; Elsliger, M. A.; Kallio, K.; Hanson, G. T.; Remington, S. J. *Struct. Fold. Des.* **1998**, *6*, 1267.
(47) Evdokimov, A. G.; Pokross, M. E.; Egorov, N. S.; Zaraisky, A. G.; Yampolsky, I. V.; Merzlyak, E. M.; Shkoporov, A. N.; Sander, I.; Lukyanov, K. A.; Chudakov, D. M. *EMBO Rep.* **2006**, *7*, 1006.
(48) Bell, A. F.; Stoner-Ma, D.; Wachter, R. M.; Tonge, P. J. *J. Am. Chem. Soc.* **2003**, *125*, 6919.
(49) Jonasson, G.; Teuler, J. M.; Vallverdu, G.; Merola, F.; Ridard, J.; Levy, B.; Demachy, I. *J. Chem. Theor. Comput.* **2011**, *7*, 1990.
(50) Pattison, D. I.; Rahmanto, A. S.; Davies, M. J. *Photochem. Photobiol. Sci.* **2012**, *11*, 38.
(51) Ochsner, M. *J. Photochem. Photobiol. B* **1997**, *39*, 1.
(52) Vogt, W. *Free Radic. Biol. Med.* **1995**, *18*, 93.
(53) Yan, P.; Xiong, Y. J.; Chen, B. W.; Negash, S.; Squier, T. C.; Mayer, M. U. *Biochemistry* **2006**, *45*, 4736.
(54) Schoneich, C. *Biochim. Biophys. Acta* **2005**, *1703*, 111.
(55) Kim, Y. H.; Berry, A. H.; Spencer, D. S.; Stites, W. E. *Protein Eng.* **2001**, *14*, 343.
(56) Alvarez, L.; Levin, C. H.; Merola, F.; Bizouarn, T.; Pasquier, H.; Baciou, L.; Rusconi, F.; Erard, M. *Photochem. Photobiol.* **2010**, *86*, 55.
(57) Langhojer, F.; Dimler, F.; Jung, G.; Brixner, T. *Biophys. J.* **2009**, *96*, 2763.
(58) Ding, L. N.; Chung, L. W.; Morokuma, K. *J. Phys. Chem. B* **2013**, *117*, 1075.
(59) Gayda, S.; Nienhaus, K.; Nienhaus, G. U. *Biophys. J.* **2012**, *103*, 2521.
(60) Dixit, R.; Cyr, R. *Plant J.* **2003**, *36*, 280.
(61) Hoebe, R. A.; Van Oven, C. H.; Gadella, T. W., Jr.; Dhonukshe, P. B.; Van Noorden, C. J.; Manders, E. M. *Nat. Biotechnol.* **2007**, *25*, 249.
(62) Shroff, H.; Galbraith, C. G.; Galbraith, J. A.; Betzig, E. *Nat. Methods* **2008**, *5*, 417.
(63) Manley, S.; Gillette, J. M.; Patterson, G. H.; Shroff, H.; Hess, H. F.; Betzig, E.; Lippincott-Schwartz, J. *Nat. Methods* **2008**, *5*, 155.
(64) Gudheti, M. V.; Curthoys, N. M.; Gould, T. J.; Kim, D.; Gunewardene, M. S.; Gabor, K. A.; Gosse, J. A.; Kim, C. H.; Zimmerberg, J.; Hess, S. T. *Biophys. J.* **2013**, *104*, 2182.
(65) Henriques, R.; Griffiths, C.; Rego, E. H.; Mhlanga, M. M. *Biopolymers* **2011**, *95*, 322.